Strong and weak second-order topological insulators with hexagonal symmetry and $\mathbb{Z}_{3}$ index

Motohiko Ezawa

Phys. Rev. B **97**, 241402 — Published 4 June 2018

DOI: 10.1103/PhysRevB.97.241402

Strong and weak second-order topological insulators with hexagonal symmetry and $\mathbb{Z}_3$ index

Motohiko Ezawa

We propose second-order topological insulators (SOTIs) whose lattice structure has the hexagonal symmetry C_6. We start with a three-dimensional weak topological insulator constructed on the stacked triangular lattice, which has only side topological surface states. We then introduce an additional mass term which gaps out the side surface states but preserves the hinge states. The resultant system is a three-dimensional SOTI. The bulk topological quantum number is shown to be the $\mathbb{Z}_3$ index protected by the inversion time-reversal symmetry IT and the rotoinversion symmetry IC_6. We obtain three phases; trivial, strong and weak SOTI phases. We argue the origin of these two types of SOTIs. A hexagonal prism is a typical structure respecting these symmetries, where six topological hinge states emerge at the side. The building block is a hexagon in two dimensions, where topological corner states emerge at the six corners in the SOTI phase. Strong and weak SOTIs are obtained when the interlayer hopping interaction is strong and weak, respectively.

Topological phase of matter remains to be a most active field of condensed matter physics. Topological insulators (TIs) are well established, where the emergence of topological boundary states is a manifestation of the bulk topological number[1,2]. This is known as the bulk-boundary correspondence. Recently, the notion of topological insulators is generalized to second-order topological insulators (SOTIs)[3–15]. A SOTI is such an insulator that has no topological surface states though it has topological hinge states. They are one-dimensional (1D) edge states emerging at hinges of a prism respecting the symmetry based upon which the bulk topological quantum number is defined.

One powerful method to create a SOTI is to introduce a mass term to a strong TI in such a way that it gaps out surface states but preserves hinge states[10]. A topological hinge insulator was first constructed[10] by applying this method to the C_4 symmetric lattice model. However, in this model[10] a tetragonal prism of finite size has gapless surface states at the top and the bottom of the prism in addition to four gapless hinge states. This is because the symmetry indicator is characterized by C_4T and $\bar{C}_4 = IC_4$, where T and I are the time-reversal symmetry generator and the inversion generator, respectively. These surface states can be gapped out[16] by introducing the Zeeman term violating C_4T but preserving $\bar{C}_4$. The bulk topological number, being characterized by the rotoinversion symmetry $\bar{C}_4$, is given by the $\mathbb{Z}_2$ index.

Very recently, by employing topological quantum chemistry for material prediction[17–22], bismuth was predicted theoretically and shown experimentally to be a SOTI[23] with a clear observation of hinges. It has the C_6 symmetric lattice structure. The tight-binding model has been proposed, but it is an eight-band model and rather too complicated. On the other hand, there is a classification of 2D topological crystalline insulators, which shows a system having six corners protected by the particle-hole symmetry[24]. For instance, the six-corner states emerge in a photonic crystal[25].

In this paper, we propose a simple four-band model possessing the C_6 symmetric lattice structure realizing a SOTI. We start with a weak TI realized on the stacked triangular lattice, whose topological surface states are present only at the side surfaces. Namely, it has no gapless surface states at the top and the bottom when we consider a hexagonal prism of finite size as in Fig.1(a). Then, we gap out the side surface states by introducing an additional mass term with parameter Δ. As a result, we obtain a SOTI, which has topological hinge states as in Fig.1(b). The bulk topological quantum number is shown to be the $\mathbb{Z}_3$ index characterized by combinations of the rotoinversion symmetry $\bar{C}_6 = IC_6$ and the inversion time-reversal symmetry IT. In accord with the $\mathbb{Z}_3$ index, there exist two different types of SOTIs. We call them strong and weak SOTIs. We also study a 2D SOTI by taking the limit of the zero interlayer hopping, where the bulk topological quantum number is given by the $\mathbb{Z}_2$ index.

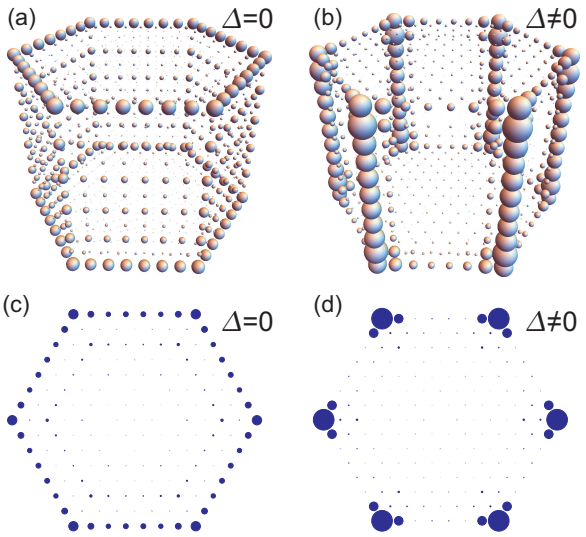

FIG. 1. (a)–(b) A hexagonal prism is a typical structure respecting the rotoinversion symmetry $\bar{C}_6$. The real-space plot of the local density ρ_i of the zero-energy states for a hexagonal prism in the case of (a) a weak TI with $\Delta = 0$ and (b) a topological hinge insulator with $\Delta = 0.7$. The amplitude is represented by the radius of spheres. The length of one side of the hexagon is $L = 8$, and the height of the prism is $H = 11$. (c)–(d) A hexagon is a typical structure respecting the rotoinversion symmetry $\bar{C}_6$. The real-space plot of ρ_i of the zero-energy states for a hexagon in the case of (c) a TI and (d) a topological corner insulator. A weak (strong) topological hinge insulator is obtained by stacking topological corner insulators when the interlayer interaction t_z is weak (strong). We have set $t = 1$, $t_z = 2$, $\lambda = \lambda_z = 1$ and $m = 3$.

Hamiltonian: We construct a weak TI realized on the

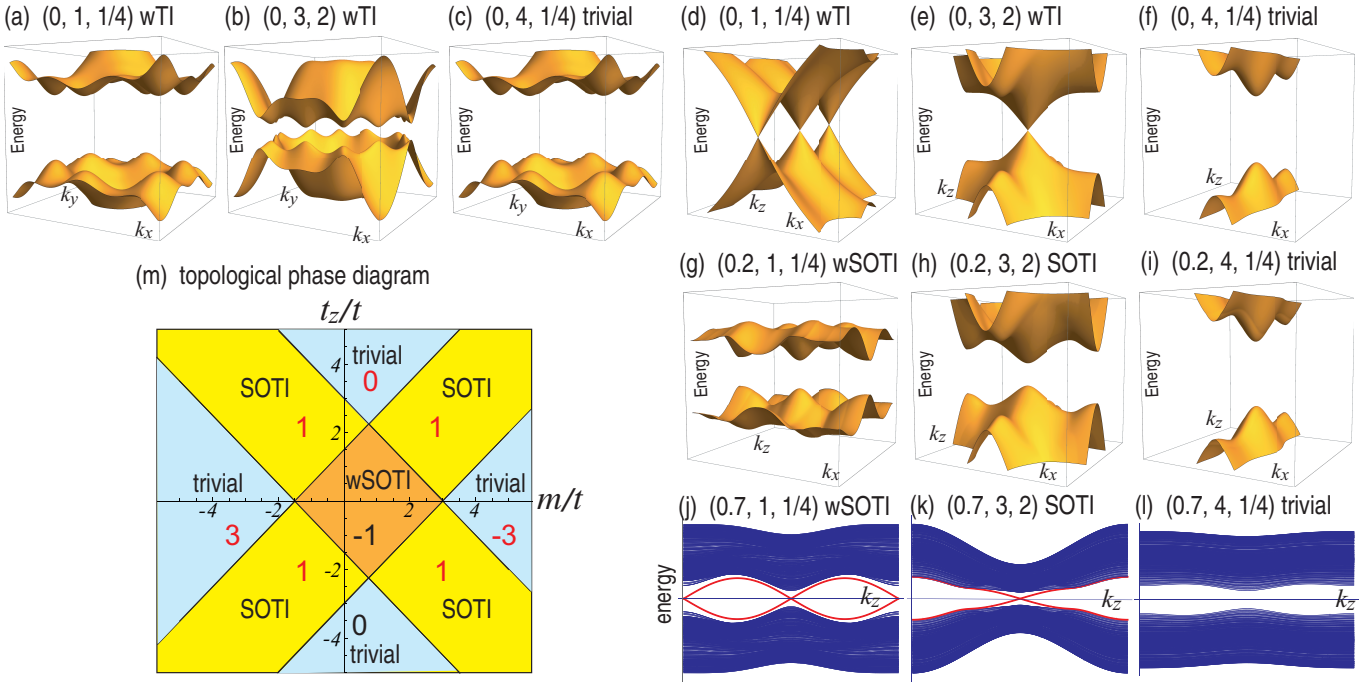

FIG. 2. (a)–(c) Band structures of top surface states in a thin film for $\Delta = 0$, where gaps are open. (d)–(f) Band structures of side surface states in a thin film for $\Delta \neq 0$. Two and one Dirac cones are observed in (d)–(e), respectively, showing the system is in the weak TI phase. A gap exists in (f), showing the system is in the trivial phase. (g)–(i) The figures corresponding to (d)–(f) for $\Delta \neq 0$, showing the weak TI phase is transformed into the SOTI phase. (j)–(l) Band structures of a hexagonal prism, where hinge states are shown in red. They are remnants of the Dirac cones observed in (d) and (e). The gap closes at two or one points in the weak or strong SOTI as in (j) or (k). Parameters (Δ, m, t_z) are displayed in figures. The other parameters are $t = 1 = \lambda = \lambda_z$=1. (m) Topological phase diagram of the 3D model. The horizontal axis is m/t, while the vertical axis is t_z/t. Numbers in red represent the symmetry indicator κ_6. The topological quantum number ν_{3D} is defined by $\nu_{3D} = \mathrm{mod}_3 \kappa_6$. Thus, there are two SOTI phases shown by $\kappa_6 = \pm 1$, corresponding to (j) and (k). It does not depend on λ, λ_z and Δ. The horizontal axis of (j)–(l) is k_z in the range of $(-\pi, \pi)$.

stacked triangular lattice. The Hamiltonian consists of the 2D Hamiltonian and the interlayer interaction terms. As the 2D Hamiltonian we take[26]

$$H^0_{2D} = H_t \tau_z + H_{SO} \tau_x \tag{1}$$

on the triangular lattice, where

$$H_t = \sum_{n=1}^{3} m - t \sum \cos\left(\mathbf{d}_n \cdot \mathbf{k}\right), \tag{2}$$

$$H_{SO} = \lambda \sum_{n=1}^{3} C_3^n \sigma_x C_3^{-n} \sin\left(\mathbf{d}_n \cdot \mathbf{k}\right) \tag{3}$$

in the momentum space. Here, m, t, λ are real parameters, $\mathbf{k} = (k_x, k_y)$, and $\mathbf{d}_n = |\mathbf{d}_n|[\cos(2\pi n/3), \sin(2\pi n/3)]$ is the pointing vector; $\sigma = (\sigma_x, \sigma_y, \sigma_z)$ and $\tau = (\tau_x, \tau_y, \tau_z)$ represent the Pauli matrices for the spin and the pseudospin corresponding to the orbital degrees of freedom, respectively; $C_3 = \tau_0 \exp\left[-i\pi\sigma_z/3\right]$ is the generator of the $\pi/3$ rotation. It has been shown[26] that the Hamiltonian H^0_{2D} describes a 2D TI. According to the bulk-boundary correspondence there emerge gapless edge states for a hexagon as in Fig.1(c).

We may stack triangular lattices to generate a 3D lattice. The 3D Hamiltonian is given by

$$H^0_{3D} = H^0_{2D} + H_z \tag{4}$$

with

$$H_z = -t_z \tau_z \cos k_z + \lambda_z \tau_x \sigma_z \sin k_z, \tag{5}$$

which is a well-known term describing interlayer hopping with real parameters t_z and the spin-orbit interaction λ_z.

We consider a hexagonal prism of finite size subject to H^0_{3D}. Provided both t_z and λ_z are small enough, since the prism is simply obtained by stacking hexagons having the density of state as in Fig.1(c), it has naturally topological surface states at the six sides but none at the top and bottom as in Fig.1(a). This remains true even if the parameters t_z and λ_z are not small based on explicit calculations. See Fig.2(a)–(c) with respect to the absence of gapless surface states at the top and the bottom. Such an insulator is called a weak TI.

The problem is how to gap out the edge (side surface) states preserving the corner (hinge) states in the 2D (3D) TI. This is the main issue of the present work. For this purpose we propose to consider the Hamiltonians

$$H_{2D} = H^0_{2D} + H_\Delta \tau_0, \quad H_{3D} = H^0_{3D} + H_\Delta \tau_0, \tag{6}$$

with

$$H_\Delta = \Delta \sum_{n=1}^{3} C_3^n \sigma_y C_3^{-n} \cos\left(\mathbf{d}_n \cdot \mathbf{k}\right), \tag{7}$$

where Δ is a real parameter. It is a hexagonal generalization of the term for the tetragonal symmetric system[10]. Our result demonstrates that the $H_\Delta \tau_0$ term transforms the weak TI into a topological hinge insulator as in Fig.1(b). We also see that it transforms the 2D TI into a topological corner insulator as in Fig.1(b), about which we discuss after the 3D model.

Topological phase diagram: We analyze the Hamiltonian H_{3D}. The band structure is obtained by diagonalizing it. The essential point is that the bulk topological quantum number is defined by the band structure at the six high-symmetry points with respect to the six-fold rotoinversion: See (15) with (14). They are $\Gamma = (0,0,0)$, $K = (4\pi/3,0,0)$, $K' = (-4\pi/3,0,0)$, $A = (0,0,\pi)$, $H = (4\pi/3,0,\pi)$, $H' = (-4\pi/3,0,\pi)$. Consequently, to determine the topological phase boundaries, it is enough to solve the zero-energy condition ($E = 0$) at these six high-symmetry points.

The energies at these points are analytically obtained as

$$E(\Gamma) = \pm(3t + t_z - m), \tag{8}$$
$$E(K) = E(K') = \pm(3t/2 - t_z + m), \tag{9}$$
$$E(A) = \pm(3t - t_z - m), \tag{10}$$
$$E(H) = E(H') = \pm(3t/2 + t_z + m). \tag{11}$$

The topological phase boundary is given by $t_z = \pm 3t + m$ and $t_z = \pm 3t/2 - m$, which are shown in Fig.2(m). They are independent of the values of $\lambda, \lambda_z, \Delta$.

Symmetries: In order to identify the bulk topological quantum number, it is necessary to study the symmetry of the Hamiltonian H_{3D}. We note that the Hamiltonian H^0_{3D} has both the time-reversal symmetry $TH^0_{3D}(\mathbf{k})T^{-1} = H^0_{3D}(-\mathbf{k})$ and the inversion symmetry $IH^0_{3D}(\mathbf{k})I^{-1} = H^0_{3D}(-\mathbf{k})$, where $T = -i\tau_0\sigma_y K$ generates the time reversal symmetry (TRS) with the complex conjugation K, while $I = \tau_z\sigma_0$ is the inversion symmetry generator. In addition, there is the six-fold rotational symmetry C_6,

$$C_6 H^0_{3D}(k_x,k_y,k_z)C_6^{-1} = H^0_{3D}(k'_x,k'_y,k_z), \tag{12}$$

where $C_6 = \tau_0 \exp[-i\pi\sigma_z/6]$ is the generator of the $\pi/6$ rotation, and

$$k'_x = k_x/2 + \sqrt{3}k_y/2, \quad k'_y = -\sqrt{3}k_x/2 + k_y/2. \tag{13}$$

The term H_Δ breaks both the TRS and the inversion symmetry but preserves the combined symmetry IT and the rotoinversion symmetry $\bar{C}_6 = IC_6$, which is similar to the case of the tetragonal system[10].

Symmetry indicator: The symmetry indicator is already known for the tetragonal system possessing the $\bar{C}_4$ and IT symmetries[10,27]. By making its hexagonal generalization, we define the symmetry indicator κ_6 protected by the $\bar{C}_6$ and IT symmetries by the formula

$$\kappa_6^{3D} = \frac{1}{2\sqrt{3}} \sum_k \sum_\alpha e^{\frac{i\alpha\pi}{6}} n_K^\alpha, \tag{14}$$

where k runs over the symmetry invariant points associated with $\bar{C}_6$, Γ, K, K', A, H and H'; n_K^α is the number of the occupied bands with the eigenvalue $e^{\frac{i\alpha\pi}{6}}$ of the symmetry operator $\bar{C}_6$, $\bar{C}_6|\psi\rangle = e^{\frac{i\alpha\pi}{6}}|\psi\rangle$. The symmetry indicator is shown

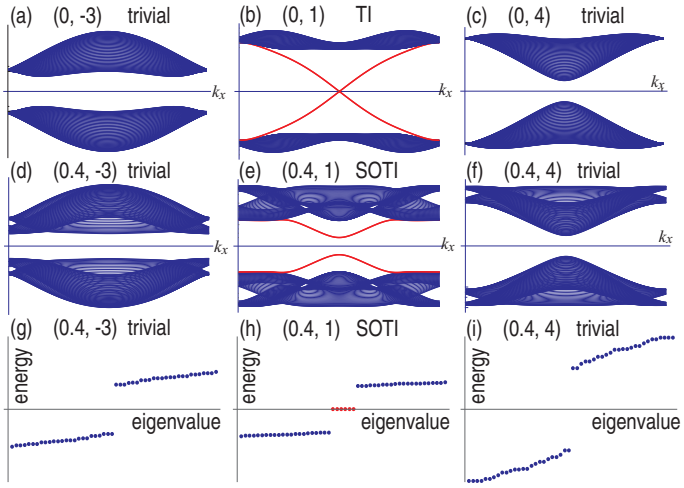

FIG. 3. Band structures of the 2D model (a)–(c) with $\Delta = 0$ and (d)–(f) with $\Delta \neq 0$ in nanoribbon geometry for typical points in the phase diagram. (g)–(i) Eigenenergy of the 2D model in hexagonal nanodisk geometry for typical points in the phase diagram. (h) Six degenerate zero-energy states emerge in the SOTI phase. Parameters (Δ, m) are displayed in figures. The horizontal axis of (a)–(f) is k_x in the range of $(-\pi, \pi)$.

to be quantized and real. First, α is quantized to be $\alpha = 1, 3, 5, 7, 9, 11$, because of the relation $(\bar{C}_6)^6 = -1$. Second, κ_6 is real, since the band structure is always two-fold degenerate in the presence of the IT symmetry. The symmetry eigenvalues form a conjugate pair[10] for these bands due to the commutation relation $[\bar{C}_6, IT] = 0$ and the fact that the IT symmetry is anti-unitary. Third, κ_6 is a constant within one topological phase since it can change its value only when a phase boundary is crossed by changing system parameters. Consequently it is a candidate of the topological quantum number. We explicitly evaluate κ_6 using the formula (14), which is shown in the phase diagram Fig.2(m).

Surface states: We first examine the surface states by analyzing the band structure of a thin film. (i) When $\Delta = 0$, gapless modes are found in the side surfaces [Fig.2(d)–(e)] in the TI phase, but not in the up and bottom surfaces [Fig.2(a)–(b)], which shows that the system is a weak TI. (ii) When $\Delta \neq 0$, these surface states are gapped [Fig.2(g)–(h)]. These features are consistent with the local density of states for the hexagonal prism as shown in Fig.1(a)–(b). Hence, the system is naively a trivial insulator according to the bulk-boundary correspondence. However, as we now see, hinge states appear, signaling that it is a SOTI.

Hinge states and $\mathbb{Z}_3$ index protected by $\bar{C}_6$ and IT: We next investigate the hinge states by analyzing the band structure of a hexagonal prism [Fig.2(j)–(l)] at various points in the phase diagram [Fig.2(m)]. According to the band structure of a hexagonal prism, hinge states emerge in the two phases indexed by $\kappa_6 = \pm 1$ as in Fig.2(j)–(k), while no hinge states are present in the phase indexed by $\kappa_6 = 0, \pm 3$ as in Fig.2(l). They are identified with SOTI and trivial phases. The two SOTI phases indexed by $\kappa_6 = \pm 1$ are distinguished by the band structure of hinge states. Namely, hinge states are de-

tached from (attached to) the bulk band, or the gap closes at two (one) points, for $\kappa_6 = -1$ ($\kappa_6 = 1$): See Fig.2(j) and (k). Consequently, the bulk topological index is given by the $\mathbb{Z}_3$ index defined by

$$\nu_{3\mathrm{D}} = \mathrm{mod}_3 \kappa_6, \tag{15}$$

which is a generalization of the $\mathbb{Z}_2$ index ν_0 to the hexagonal symmetric system in the absence of the TRS and the inversion symmetry.

It is intriguing that we have two different types of hinge states. We may understand their origin as follows. Recall that the hexagonal prism is described by the Hamiltonian $H_{3\mathrm{D}} = H_{2\mathrm{D}} + H_z$. The building block of a hexagonal prism is a hexagon described by $H_{2\mathrm{D}}$. As we soon discuss, it has six detached corner states protected topologically, as shown in Fig.1(d). Hence, when we construct a prism by stacking hexagons, we would obtain a perfect flat band for the hinge states in the vanishing limit of interlayer hopping ($H_z \to 0$). On the other hand, when the interlayer hopping interaction t_z is strong, a mixing occurs between $H_{2\mathrm{D}}$ and H_z, making the corner states a part of the bulk bands. The resultant hinge states form the SOTI phase with $\kappa_6 = 1$, which we call a strong SOTI phase.

We proceed to study the perturbation effects on hinge states by applying the interaction of the form $H_{\alpha\beta} = B\tau_\alpha\sigma_\beta$. The results read that the hinge states split when both the rotoinversion symmetry $\bar{C}_6$ and the inversion time-reversal symmetry IT are broken. See Supplementary Materials for details[28].

2D SOTI: We analyze a hexagonal SOTI model in two dimensions. The Hamiltonian is $H_{2\mathrm{D}}$ given by (6). There is an additional chiral symmetry $CH_{2\mathrm{D}}(\mathbf{k})C^{-1} = -H_{2\mathrm{D}}(\mathbf{k})$ with the chiral symmetry operator $C = \tau_x\sigma_z$. The properties of the 2D hexagonal SOTI are summarized as follows.

First, the topological phase diagram is obtained by setting $t_z = 0$ in Fig.2(m). Namely, there emerge a SOTI phase for $-3/2 < m/t < 3$, and trivial phases for $m/t < -3/2$ and $m/t > 3$. There are only two phases for $t_z = 0$. We will soon see that the topological number is $\mathbb{Z}_2$ in the 2D SOTI, which is contrasted with the $\mathbb{Z}_3$ index in the 3D SOTI.

Second, we investigate the topological index. We start with the symmetry indicator (14) protected by the $\bar{C}_6$ and IT symmetries in a slightly modified form,

$$\kappa_6^{2\mathrm{D}} = \frac{1}{\sqrt{3}} \sum_k \sum_\alpha e^{\frac{i\alpha\pi}{6}} n_K^\alpha, \tag{16}$$

where k runs over Γ, K and K', and the prefactor is doubled since the number of the high-symmetry points in the 2D model is three instead of six in the 3D model. It follows that $\kappa_6^{2\mathrm{D}} = 3$ for $m/t < -3/2$, $\kappa_6^{2\mathrm{D}} = -1$ for $-3/2 < m/t < 1$ and $\kappa_6^{2\mathrm{D}} = -3$ for $m/t > 3$. The topological phase transition occurs at $m/t = -3/2$ ($m/t = 3$) because the band inversion occurs at the Γ point (K and K' points).

As we have noticed, there are only one kind of topological phase: See the phase diagram Fig.2(m). Hence, the 2D SOTI is characterized by the $\mathbb{Z}_2$ index. Accordingly we define the bulk topological quantum number by

$$\nu_{2\mathrm{D}} = \mathrm{mod}_2(\mathrm{mod}_3(-\kappa_6^{2\mathrm{D}})). \tag{17}$$

It follows that $\nu_{2\mathrm{D}} = 0$ for $m/t < -3/2$ and $m/t > 3$ and $\nu_{2\mathrm{D}} = 1$ for $-3/2 < m/t < 1$. We note that the notion of the strong or weak can only be applied for the hinge states.

Third, we show the band structure of a nanoribbon in Fig.3(a)–(f). When $\Delta = 0$, there are helical edge states in Fig.3(b). We have previously shown[26] that the system is a TI. They are gapped for $\Delta \neq 0$ as in Fig.3(e), indicating that the system would be topologically trivial. Actually, it is not trivial but it is in the SOTI phase.

Forth, we show the band structure of a hexagonal nanodisk in Fig.3(g)–(i) for $\Delta \neq 0$. Six-fold degenerate zero-energy corner states emerge for the SOTI phase as in Fig.3(h), showing the system is a topological corner insulator as in Fig.1(d). These zero-energy corner states are protected by the chiral symmetry C.

Finally, we study the finite-size effect on the eigenenergies of a hexagonal nanodisk. When the size is reasonably large, the spectrum forms a continuous line across the Fermi level for $\Delta = 0$, while the six corner states are fixed at zero energy for $\Delta \neq 0$. We also study the perturbation effects of the form $H_{\alpha\beta} = B\tau_\alpha\sigma_\beta$. The corner states remain as they are as long as the chiral symmetry is intact. See Supplementary Material for details[28].

In this work we have presented a simple model for a hexagonal topological hinge insulator. Although the hinge structure at the sides looks the same as that of bismuth, there are some difference between them. Indeed, the topological quantum number is the $\mathbb{Z}_3$ index in the present model but it is the $\mathbb{Z}_2$ index in the bismuth model. The origin of the difference is traced back to the fact that a hexagonal prism is constructed by stacking hexagons which are weak TIs. It yields two types of SOTIs depending on the interlayer hopping interaction whether it is strong or weak.

The author is very much grateful to B. A. Bernevig, T. Neupert and N. Nagaosa for helpful discussions on the subject. This work is supported by the Grants-in-Aid for Scientific Research from MEXT KAKENHI (Grant Nos.JP17K05490, JP15H05854 and 18H03676). This work is also supported by CREST, JST (JPMJCR16F1).

[1] M. Z. Hasan and C. L. Kane, Rev. Mod. Phys. **82**, 3045 (2010).
[2] X.-L. Qi and S.-C. Zhang, Rev. Mod. Phys. **83**, 1057 (2011).
[3] F. Zhang, C.L. Kane and E.J. Mele, Phys. Rev. Lett. **110**, 046404 (2013).
[4] W. A. Benalcazar, B. A. Bernevig, and T. L. Hughes, 10.1126/science.aah6442.
[5] F. Schindler, A. Cook, M. G. Vergniory, and T. Neupert, in APS March Meeting (2017).
[6] Y. Peng, Y. Bao, and F. von Oppen, Phys. Rev. B **95**, 235143 (2017).

[7] J. Langbehn, Y. Peng, L. Trifunovic, F. von Oppen, and P. W. Brouwer, Phys. Rev. Lett. **119**, 246401 (2017).

[8] Z. Song, Z. Fang, and C. Fang, Phys. Rev. Lett. **119**, 246402 (2017).

[9] W. A. Benalcazar, B. A. Bernevig, and T. L. Hughes, Phys. Rev. B **96**, 245115 (2017).

[10] F. Schindler, A. M. Cook, M. G. Vergniory, Z. Wang, S. S. P. Parkin, B. A. Bernevig, and T. Neupert, cond-mat/arXiv:1708.03636 (2017). .

[11] C. Fang, L. Fu, arXiv:1709.01929

[12] M. Ezawa, Phys. Rev. Lett. 120, 026801 (2018)

[13] M. Ezawa, cond-mat/arXiv:1801.00437.

[14] M. Geier, L. Trifunovic, M. Hoskam, and P. W. Brouwer, cond-mat/arXiv:1801.10053

[15] E. Khalaf, cond-mat/arXiv:1801.10050

[16] M. Ezawa, cond-mat/arXiv:1802.03571.

[17] B. Bradlyn, L. Elcoro, J. Cano, M. G. Vergniory, Z. Wang, C. Felser, M. I. Aroyo, and B. A. Bernevig, Nature 547, 298 (2017).

[18] M. G. Vergniory, L. Elcoro, Z. Wang, J. Cano, C. Felser, M. I.Aroyo, B. A. Bernevig, and B. Bradlyn, Phys. Rev. E 96, 023310 (2017).

[19] L. Elcoro, B. Bradlyn, Z. Wang, M. G. Vergniory, J. Cano, C. Felser, B. A. Bernevig, D. Orobengoa, G. Flor, and M. I. Aroyo, Journal of Applied Crystallography 50 (2017).

[20] J. Cano, B. Bradlyn, Z. Wang, L. Elcoro, M. G. Vergniory, C. Felser, M. I. Aroyo, and B. A. Bernevig, cond-mat/arXiv:1709.01935

[21] B. Bradlyn, L. Elcoro, M. G. Vergniory, J. Cano, Z. Wang, C. Felser, M. I. Aroyo, and B. A. Bernevig, ArXiv e-prints (2017), cond-mat/arXiv:1709.01937

[22] J. Cano, B. Bradlyn, Z. Wang, L. Elcoro, M. G. Vergniory, C. Felser, M. I. Aroyo, and B. A. Bernevig, cond-mat/arXiv:1711.11045

[23] F. Schindler, Z. Wang, M. G. Vergniory, A. M. Cook, A. Murani, S. Sengupta, A. Y. Kasumov, R. Deblock, S. Jeon, I. Drozdov, H. Bouchiat, S. Gueon, A. Yazdani, B. A. Bernevig, and T. Neupert, cond-mat/arXiv:1802.02585.

[24] Wladimir A. Benalcazar, Jeffrey C. Y. Teo, and Taylor L. Hughes, Phys. Rev. B 89, 224503 (2014)

[25] Jiho Noh, Wladimir A. Benalcazar, Sheng Huang, Matthew J. Collins, Kevin Chen, Taylor L. Hughes, Mikael C. Rechtsman, arXiv:1611.02373

[26] M. Ezawa, New J. Phys. 16, 065015 (2014).

[27] E. Khalaf, H. C. Po, A. Vishwanath and H. Watanabe, cond-mat/arXiv:1711.11589.

[28] See Supplemental Material at [URL]. Here we study the perturbation effects both on hinge states and corner states by applying the interaction of the form $H_{\alpha\beta} = B\tau_\alpha\sigma_\beta$.